Table 1. Missense mutations of PI3K isoforms, *PTEN*, *KRAS*, and *BRAF* in JFCR39

ID	Origin	Cell line	*PIK3CA*	*PIK3CB*	*PIK3CD*	*PIK3CG*	*PTEN*	*KRAS*	*BRAF*
01	Lung ca.	NCI-H23				P538L		G12C	
02		NCI-H226				S442Y (SNP)			
03		NCI-H522							
04		NCI-H460	E545K (genomic)					Q61H	
05		A549						G12S	
06		DMS273				M259I	K128N		
07		DMS114							
11	Colorectal ca.	HCC2998	I391M (SNP)	R149Q		T857A	Y46C	A146T	
				R562Q		R273H	R130Q		
						L466M	F341V		
12		KM-12					G129* K267fs(del.-1)*9		
13		HT-29	P449T			S442Y(SNP)			V600E
15		HCT-15	E545K D549N	R628Q	S174L			G13D	
16		HCT-116	H1047R		Ex.16 del.		G13D		
21	Gastric ca.	St-4				S442Y(SNP)	E291*	G12A	
22		MKN1	E545K						
23		MKN7			T456A (SNP)	A621S			
24		MKN28			T456A (SNP)	A621S			
25		MKN45							
26		MKN74			T456A (SNP)	A621S			
31	Breast ca.	HBC-4		E1051K		S442Y(SNP)			
32		BSY-1	H1047R				Ex.1-9 del.		
34		HBC-5							
35		MCF-7	E545K			S442Y(SNP)			
36		MDA-MB-231						G13D	G464V
41	Ovarian ca.	OVCAR-3							
42		OVCAR-4							
43		OVCAR-5						G12V	
44		OVCAR-8				N522S			
45		SK-OV-3	H1047R						
51	Brain ca.	U251					E242fs(ins.+2)*15		
52		SF-268							
53		SF-295			S312C		R233*		
54		SF-539					Ex.1-9 del.		
55		SNB-75							
56		SNB-78	L719F				T26fs(SD del.)		
61	Renal ca.	RXF-631L				S442Y(SNP)			
62		ACHN							
71	Melanoma	LOX-IMVI							V600E
91	Prostate ca.	DU-145		A686T		S442Y(SNP)			
92		PC-3			S312C	S442Y(SNP)	Ex.3-9 del.		
Total # (without SNP)			10 (9)	4	7 (4)	15 (7)	10	9	3

NOTE: Underline indicates a homozygous mutation.

Drugs

ZSTK474 was kindly provided by Zenyaku Kogyo Co. Ltd. LY294002, PI103, PI3Kα inhibitor IV, PI3Kγ inhibitor (AS605240), and Akt inhibitors II, III, IV, V (triciribine), VIII, IX, X, and XI were purchased from Calbiochem. TGX221 and perifosine were purchased from Cayman. GDC-0941 and IC87114 were obtained from Symansis. RAD001 and CCI779 were purchased from LC Laboratories. Wortmannin,

PX-866, NVP-BEZ235, and rapamycin were obtained from Kyowa Medex, Sigma, Selleck, and Wako Pure Chemical, respectively.

Determination of drug efficacy

Drug efficacy was assessed as changes in total cellular protein after 48 hours of drug treatment using a sulforhodamine B assay. Assays were done in duplicate and the GI_{50} was calculated as described previously (27, 33).

Animal experiments

Animal care and treatment were done in accordance with the guidelines of the animal use and care committee of the Japanese Foundation for Cancer Research and conformed to the NIH Guide for the Care and Use of Laboratory Animals. Female nude mice with BALB/c genetic backgrounds were purchased from Charles River Japan. Mice were maintained under specific pathogen-free conditions and provided with sterile food and water *ad libitum*. Human tumor xenografts were generated by s.c. inoculating nude mice with 3 mm × 3 mm × 3 mm tumor fragments of human cancer cells. When the tumors became 100 to 300 mm^3 in size, ZSTK474 was p.o. administered at 100, 200, and 400 mg/kg of body weight following the indicated schedule. The length (L) and width (W) of the subcutaneous tumor mass were measured by calipers in live mice, and the tumor volume (TV) was calculated as $TV = (L \times W^2)/2$. Percent treated/control [T/C (%)] was calculated as $(TV_{with\ drug}/TV_{control}) \times 100$. To assess toxicity, we measured the body weight of the tumor-bearing mice. Mice were finally sacrificed and tumors were excised and frozen in liquid N_2.

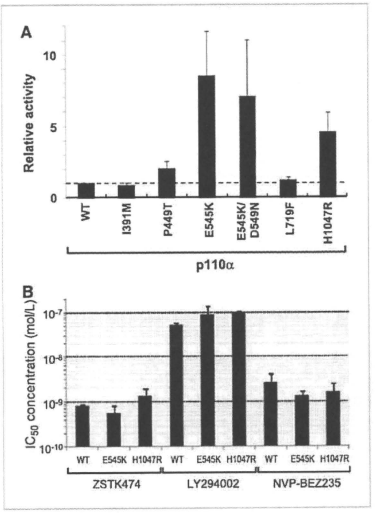

Figure 1. Relative kinase activities of p110α mutants and the inhibitory effect of PI3K inhibitors against hotspot mutants of p110α. A, recombinant FLAG-tagged PI3K p110α/p85α protein complex produced in 293T cells was immunoprecipitated, and the immunoprecipitates were used for the quantitative PI3K-HTRF assay (32). B, effect of three PI3K inhibitors (ZSTK474, LY294002, and NVP-BEZ235) on the enzymatic activity of two hotspot mutants (E545K and H1047R) p110α compared with the wild-type. No striking difference was observed in the IC_{50} concentrations of these inhibitors between wild-type and mutant p110α.

Results

Characterization of the mutation status of PIK3Cs, PTEN, KRAS, and BRAF in JFCR39 cell lines

We first examined the mutation status of PI3K isoforms in the JFCR39 cell lines (Table 1; Supplementary Table S2). Analysis of genomic sequences of *PIK3CA* on exon 9 and exon 20 revealed the hotspot mutations (E545K in four cell lines and H1047R in three cell lines). Analysis of the full coding sequence of cDNA revealed four additional missense mutations: I391M, P449T, D549N, and L719F. Evaluation of relative kinase activity of these mutants revealed that mutant P449T exhibited gain of function (>2-fold) compared with wild-type PI3Kα (Fig. 1A). The E545K mutation found in NCI-H460 genomic DNA was not detected in the cDNA, suggesting that the allele with the E545K mutation was hardly transcribed in NCI-H460 cells. Therefore, we concluded that seven cell lines [HCT-116, SK-OV3, BSY-1 (H1047R), MKN-1, MCF7 (E545K), HCT-15 (E545K/D549N), and HT-29 (P449T)] expressed a gain-of-function mutant of *PIK3CA*. With regard to two hotspot mutants (E545K and H1047R), we examined the effect of three representative PI3K inhibitors on their enzymatic activity and found no striking difference in their efficacies compared with wild-type p110α (Fig. 1B).

In addition to *PIK3CA*, we examined the genomic sequences of all coding exons of *PIK3CB*, *PIK3CD*, and *PIK3CG* genes and found five missense mutations in *PIK3CB*, three in *PIK3CD*, and eight in *PIK3CG* (Table 1; Supplementary Table S2). Most of these mutations were not registered in the dbSNP database established by The National Center for Biotechnology Information. Therefore, this study is the first report showing that cancer cells harbor missense mutations in *PIK3CB*, *PIK3CG*, and *PIK3CD* as well as in *PIK3CA*.

Next, we proceeded to examine the genomic sequences of the *PTEN* gene and found that the *PTEN* gene was deleted in three cell lines (BSY-1, SF539, and PC-3), and seven had missense or frameshift mutations.

We examined the genomic sequences of exon 1 (including G12 and G13) and exon 2 (Q61) of *KRAS* and exon 15 (V600) and exon 11 (G464, G466, and G468) of *BRAF* (Table 1). Eight of 39 cell lines had a hotspot mutation in the G12, G13, or Q61 residue. On the other hand, the *BRAF* mutation was observed in three cell lines including LOX-IMV1.

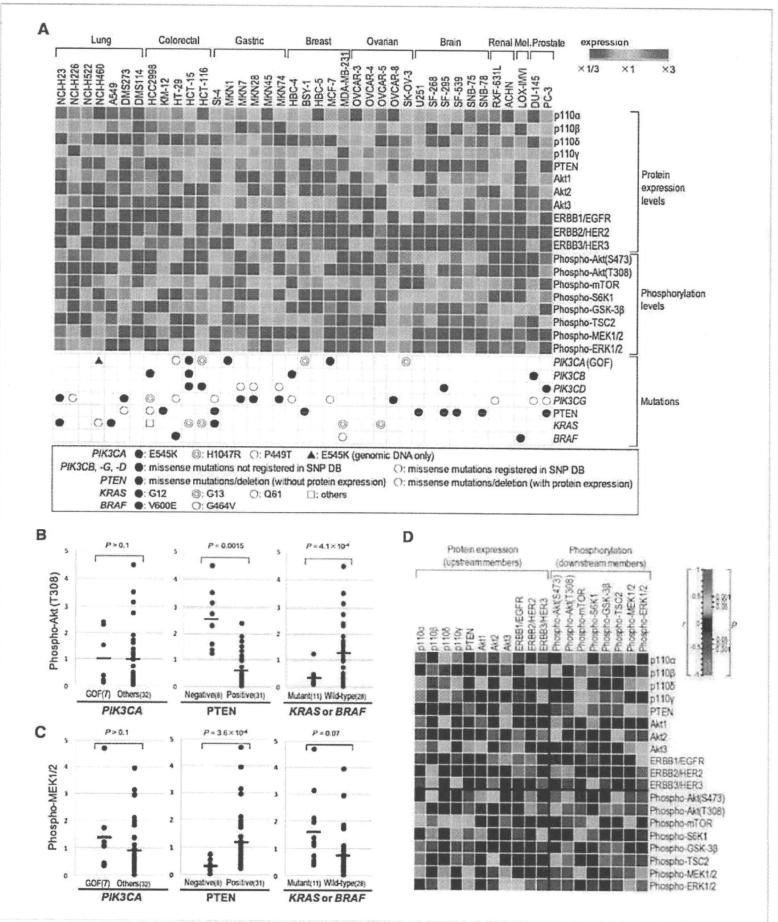

Figure 2. Mutation, protein expression, and phosphorylation status of PI3K and Ras pathway members and the correlation among them. A, the protein expression of upstream members and the phosphorylation of downstream members in each of the JFCR39 cell lines were determined by immunoblot analysis and normalized so that their average across the JFCR39 cell lines was 1 (yellow). A red point and a blue point represent high and low expression by 3-fold, respectively. Mutation data are from Table 1. B and C, differences in expression levels of phospho-Akt (T308) (B) and phospho-MEK1/2 (C) between cell lines with or without *PIK3CA* gain-of-function mutation (GOF), PTEN expression, and *KRAS*/*BRAF* mutation. Student's *t* tests were used to examine significance of differential expression. D, a heat map representing the similarities among the fingerprints of PI3K pathway members. Red to yellow: significant positive correlation ($P < 0.05$); yellow to black, black to blue: no significant correlation ($P > 0.05$), blue to sky blue: significant negative correlation ($P < 0.05$).

Expression of PI3K isoforms, PTEN, Akt isoforms, and ERBB-family RTKs

We next examined the protein expression of upstream members of the PI3K pathway that would affect downstream activity, including PI3K isoforms (p110α/β/γ/δ), PTEN, Akt isoforms (Akt1/2/3), and ERBB-family RTKs (EGFR/ERBB2/ERBB3; Fig. 2A; Supplementary Data). As expected, p110α and p110β were widely expressed, whereas p110γ and p110δ, which were thought to be expressed preferentially in leukocytes, were unexpectedly expressed in most JFCR39 cell lines derived from solid tumors. PTEN expression was undetectable in all of three cell lines with the deletion and in five of seven cell lines with a mutation, whereas all of 29 cell lines lacking a mutation or deletion expressed a certain amount of PTEN protein (Supplementary Fig. S1). Some of the cell lines exhibited overexpression of Akt isoforms; SF268 and MCF-7 highly expressed Akt1, whereas OVCAR3 and HBC5 highly expressed Akt2. EGFR was expressed in a wide variety of cell lines, but in some cell lines including NCI-H522 and MCF-7, EGFR expression was absent or present at an extremely low level. ERBB3 was highly expressed in a wide variety of cell lines derived from ovarian, gastric, breast, and colorectal cancer cell lines, but not in most brain cancer cell lines. On the other hand, ERBB2 was highly expressed in two cell lines (SK-OV-3 and HBC5).

Activation status of downstream members of the PI3K pathway

We examined the phosphorylation levels of PI3K downstream effectors including Akt (phosphorylated on T308 and S473), mTOR (S2448), S6K1 (T389), GSK-3β (S9), and TSC2 (T1462; Fig. 2A). We also examined Ras downstream effectors, phosphorylated MEK1/2 (S217/S221) and ERK1/2 (T202/Y204). Interestingly, the expression pattern of phosphorylated Akt (T308) was highly correlated with phosphorylated TSC2 ($r = 0.70$) and GSK-3β ($r = 0.60$), but not with phosphorylated mTOR and S6K1 (Fig. 2A; Supplementary Fig. S2). On the other hand, expression levels of phosphorylated Akt (T308) had a significant negative correlation with phosphorylated ERK1/2 ($r = 0.39$).

Correlation between upstream abnormalities and phosphorylation of downstream effectors in the PI3K pathway

Correlation analysis between upstream abnormalities and downstream activities revealed some interesting results (Fig. 2B and C; Supplementary Table S3). For example, phosphorylation levels of Akt (T308) ($P = 0.0015$) and TSC2 ($P = 0.011$) were significantly higher and those of MEK1/2 ($P = 3.6 \times 10^{-4}$) and ERK1/2 ($P = 2.7 \times 10^{-5}$) were significantly lower in eight PTEN-negative cell lines than those in 31 PTEN-expressing cell lines. This suggested that PTEN loss conferred activation of PI3K downstream factors and inactivation of the MAPK pathway. In contrast, phosphorylation levels of Akt (T308) ($P = 4.1 \times 10^{-4}$) and TSC2 ($P = 0.0021$) were significantly lower in cell lines having a mutation in either the *KRAS* or the *BRAF* gene, suggesting inactivation of the PI3K/Akt pathway in these cell lines. However, mutation of *PIK3CA* did not have significant associations with downstream activation, including phosphorylation levels of Akt and MEK.

Determination of efficacy patterns of 25 PI3K pathway inhibitors across JFCR39 cell lines, or fingerprints, and evaluation of their modes of action from their fingerprints

We next examined the efficacy of 25 PI3K pathway inhibitors (Table 2) in each of the JFCR39 cell lines. Then, we compared the fingerprints of PI3K inhibitors with those of other conventional anticancer drugs by cluster analysis (Fig. 3A; Supplementary Fig. S3A). Interestingly, 10 of 11 PI3K inhibitors were tightly clustered and the cluster also included Akt inhibitor VIII (AKTi-1/2) and rapamycins, suggesting similarity in the mechanisms of action across these compounds. Moreover, their fingerprints were clearly different from those of the remainder of the 10 Akt inhibitors, all of three MEK inhibitors, and other conventional anticancer drugs. Furthermore, comparison of the fingerprints of 15 PI3K pathway inhibitors in the cluster revealed that some pairs, including ZSTK474/GDC-0941 ($r = 0.86$), wortmannin/PX-866 ($r = 0.81$), and PI103/PI3Kα inhibitor IV ($r = 0.80$), exhibited extremely high correlations, suggesting a close similarity in the molecular mechanisms of action between each pair of compounds (Supplementary Fig. S3B–D).

Construction of an integrated database and correlations between the status of pathway members and the efficacy of PI3K inhibitors

We have thus far studied the drug efficacy data and the signal pathway data with regard to JFCR39 cell lines. We then combined these data to develop an integrated database (JFCR39-DB). Using JFCR39-DB, we studied the relationship between the activation status of the PI3K pathway and the efficacy of PI3K pathway inhibitors. First, we examined the correlation between the mutation status of upstream members and drug efficacy. The Student t test revealed no significant differences in the efficacies of all of 25 PI3K pathway inhibitors examined, in seven cell lines expressing a gain-of-function mutant of PI3Kα, and in the remainder of the 32 cell lines (Fig. 3B; Supplementary Table S4). As mentioned before, we examined the effect of three representative PI3K inhibitors on the enzymatic activity of two hotspot mutants of PI3Kα and found no striking difference in their efficacies compared with wild-type p110α (Fig. 1B). These results suggest that cancer cells expressing mutant PI3Kα are susceptible to PI3K inhibitors to a similar extent as those expressing wild-type PI3Kα. Moreover, PTEN status did not correlate with the efficacy of PI3K pathway inhibitors. In addition, the mutation status of other PI3K isoforms did not exhibit striking correlations either. On the other hand, cell lines having a mutation in either *KRAS* or *BRAF* exhibited resistance to several PI3K pathway inhibitors including ZSTK474 (Fig. 3B; Supplementary Table S4). The present results suggest that *KRAS/BRAF*

Table 2. The 25 PI3K pathway inhibitors used in this study and their profiles and structures (15–18)

PI3K inhibitors

ZSTK474 (4.8×10^{-7} mol/L) Selective PI3K inhibitor Preclinical	Wortmannin (9.7×10^{-6} mol/L) PI3K/mTOR/MLCK inhibitor Preclinical	LY294002 (8.1×10^{-6} mol/L) PI3K/mTOR/CK2 inhibitor Preclinical
PI103 (1.8×10^{-7} mol/L) PI3K/mTOR inhibitor Preclinical	PX866 (1.4×10^{-6} mol/L) PI3Kα/δ/γ inhibitor; derivative of wortmannin Phase I	NVP-BEZ235 (8.6×10^{-9} mol/L) PI3K/mTOR inhibitor Phase I/II
GDC-0941 (5.0×10^{-7} mol/L) Selective PI3K inhibitor Phase I	PI3Kα inhibitor IV (1.0×10^{-6} mol/L) PI3Kα/β inhibitor; derivative of PI103 Preclinical	TGX221 (1.0×10^{-5} mol/L) Selective PI3Kβ inhibitor Preclinical
IC87114 (CAL-101; 8.3×10^{-5} mol/L) Selective PI3Kδ inhibitor Phase I	AS605240 (PI3Kγ inhibitor; 9.5×10^{-6} mol/L) Selective PI3Kγ inhibitor Preclinical	

Akt inhibitors

Deguelin (7.6×10^{-6} mol/L) Selective Akt inhibitor; derivative of rotenone Preclinical	Perifosine (9.1×10^{-6} mol/L) Lipid-based PI analogue Phase II	Akt inhibitor (1.3×10^{-5} mol/L) Lipid-based PI analogue Preclinical
Akt inhibitor II (8.6×10^{-6} mol/L) Lipid-based PI analogue Preclinical	Akt inhibitor III (1.9×10^{-5} mol/L) Lipid-based PI analogue Preclinical	Akt inhibitor IV (2.8×10^{-7} mol/L) Preclinical
Akt inhibitor V (triciribine/ VQD-002; 2.2×10^{-5} mol/L) Tricyclic nucleotide Phase I/II (as triciribine phosphate)	Akt inhibitor VIII (AKTi-1/2; 8.6×10^{-6} mol/L) Allosteric Akt1/2 inhibitor Preclinical	Akt inhibitor IX (8.0×10^{-7} mol/L) Preclinical

(*Continued on the following page*)

Table 2. The 25 PI3K pathway inhibitors used in this study and their profiles and structures (15–18) (Cont'd)

Akt inhibitors

Akt inhibitor X (3.6×10^{-6} mol/L) Preclinical	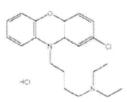	Akt inhibitor XI (1.1×10^{-5} mol/L) Preclinical 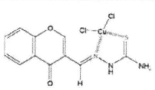

mTOR inhibitors

Rapamycin (1.7×10^{-7} mol/L) Allosteric inhibitor of mTORC1 In clinical use	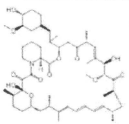	Everolimus (RAD001; 3.6×10^{-8} mol/L) Rapalogue In clinical use	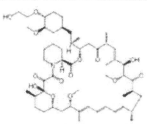	Temsirolimus (CCI779; 2.0×10^{-7} mol/L) Rapalogue In clinical use	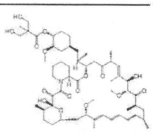

NOTE: Numbers in parentheses are mean GI_{50} values across the JFCR39 cell lines.

mutation would be a biomarker for resistance to these PI3K pathway inhibitors.

Correlation of the efficacy of PI3K pathway inhibitors with protein expression levels of PI3K isoforms, Akt isoforms, and ERBB-family RTKs

We next correlated the expression levels of the above proteins with the efficacy of PI3K pathway inhibitors (Fig. 3A). As a result, we found that expression of p110α had a slight positive correlation with four PI3K inhibitors including IC87114 and LY294002. As for p110β, we found that its high expression correlated with the efficacy of several Akt inhibitors including perifosine. As for Akt isoforms, we found that high expression of Akt2 was associated with the efficacy of five PI3K pathway inhibitors including TGX-221 and LY294002. Correlation analysis between the expression levels of ERBB-family RTKs and the efficacy of PI3K inhibitors revealed no significant correlations with PI3K pathway inhibitors. However, high expression of EGFR correlated with resistance to other classes of anticancer drugs such as navelbine ($r = -0.49$) and mitoxantrone ($r = -0.43$), suggesting that EGFR would confer resistance to these drugs in cancer cells.

Correlation of the efficacy of PI3K pathway inhibitors with phosphorylation levels of the PI3K/Akt and Ras/MAPK pathways

Lastly, we correlated the phosphorylation levels of downstream members of the PI3K pathway with drug efficacy (Fig. 3A). Of note, expression of Akt phosphorylated at S473 had significant correlations with 11 of 25 inhibitors including ZSTK474 ($r = 0.44$; Fig. 3C) and wortmannin ($r = 0.52$). In addition, phosphorylated TSC2 correlated with 7 of 25 inhibitors, including Akt inhibitor IX ($r = 0.41$) and CCI779 ($r = 0.40$). This result suggests that expression levels of Akt phosphorylated at S473 and phosphorylated TSC2 would be predictive markers for these PI3K pathway inhibitors.

Phosphorylated Akt levels and KRAS/BRAF mutation correlated with the *in vivo* efficacy of ZSTK474

We have thus far studied correlations between the status of pathway members and the efficacy of PI3K inhibitors *in vitro*. The most prominent associations were that phosphorylated Akt correlated with the efficacy whereas *KRAS/BRAF* mutation correlated with the inefficacy of PI3K inhibitors including ZSTK474. To test these correlations *in vivo*, we inoculated 24 transplantable cell lines of JFCR39 and examined the antitumor effect of ZSTK474 (Supplementary Fig. S4). We first confirmed that the *in vitro* efficacy pattern across the 24 cell lines significantly correlated with the *in vivo* efficacy pattern (200 mg/kg; $P = 0.02$), suggesting that the *in vivo* efficacy of ZSTK474 reflected its *in vitro* efficacy (Supplementary Fig. S5). Based on these data, we examined the involvement of phosphorylated Akt and *KRAS/BRAF* mutation in the efficacy of ZSTK474 *in vivo* (Fig. 4). The Student *t* test revealed that cell lines having a hotspot mutation in either *KRAS* (G12, G13, and Q61) or *BRAF* (V600) exhibited inefficacy of ZSTK474 ($P = 0.04$; Fig. 4B). Cell lines with PTEN loss such as PC-3 and BSY-1 exhibited susceptibility to ZSTK474, but the difference was not statistically significant across the 24 cell lines. On the other hand, expression levels of phosphorylated Akt in the xenografted tumors significantly correlated with susceptibility to ZSTK474 (Fig. 4C). These results suggest that phosphorylated Akt and *KRAS/BRAF* hotspot mutation could be used as a biomarker for predicting the efficacy of PI3K inhibitors in the clinic.

Discussion

In this study, taking advantage of the JFCR39 cell line panel, we examined the drug efficacy of PI3K pathway inhibitors as well as the status of PI3K and Ras pathway members, and combined them to develop an integrated database. This

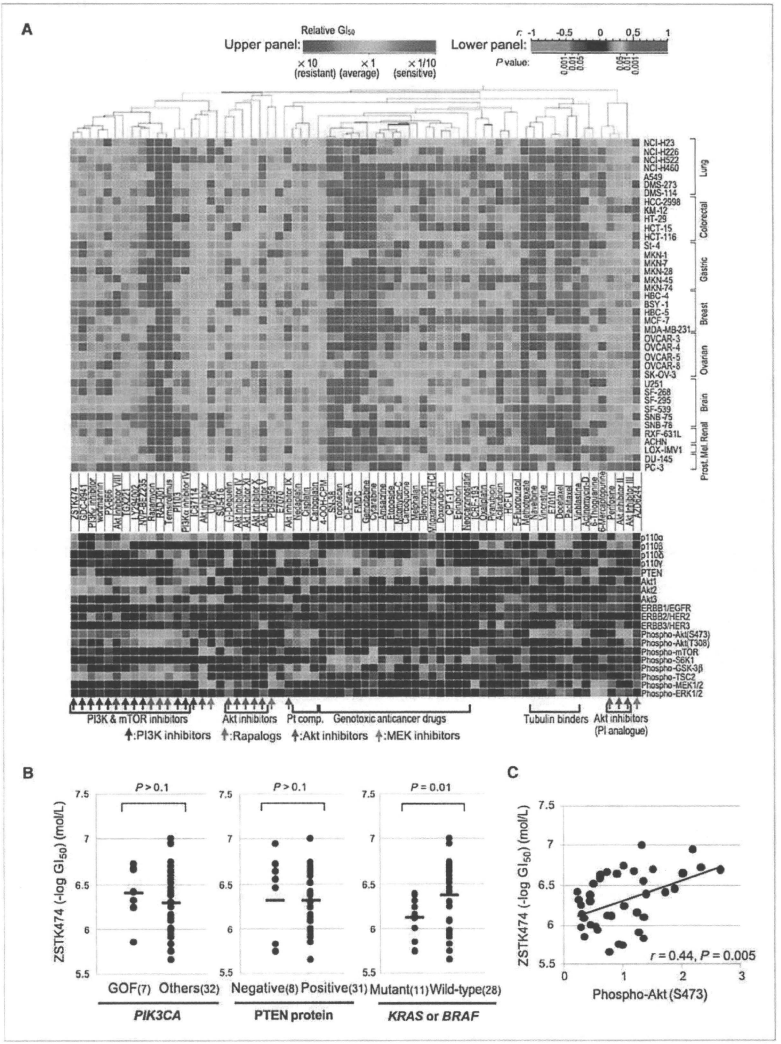
A
Relative GI50
Upper panel:
×10 (resistant)
×1 (average)
×1/10 (sensitive)
Lower panel:
r: -1 -0.5 0 0.5 1
P value:
0.001
0.01
0.05
0.05
0.01
0.001
NCI-H23
NCI-H226
NCI-H522
NCI-H460
A549
DMS-273
DMS-114
HCC-2998
KM-12
HT-29
HCT-15
HCT-116
SW-4
MKN-1
MKN-7
MKN-28
MKN-45
MKN-74
HBC-4
BSY-1
HBC-5
MCF-7
MDA-MB-231
OVCAR-3
OVCAR-4
OVCAR-5
OVCAR-8
SK-OV-3
U251
SF-268
SF-295
SF-539
SNB-75
SNB-78
RXF-631L
ACHN
LOX-IMVI
DU-145
PC-3
Lung
Colorectal
Gastric
Breast
Ovarian
Brain
Renal
Prost.
Mel.
p110α
p110β
p110δ
p110γ
PTEN
Akt1
Akt2
Akt3
ERBB1/EGFR
ERBB2/HER2
ERBB3/HER3
Phospho-Akt(S473)
Phospho-Akt(T308)
Phospho-mTOR
Phospho-S6K1
Phospho-GSK-3β
Phospho-TSC2
Phospho-MEK1/2
Phospho-ERK1/2
PI3K & mTOR inhibitors
Akt inhibitors
Pt comp.
Genotoxic anticancer drugs
Tubulin binders
Akt inhibitors (PI analogue)
:PI3K inhibitors
:Rapalogs
:Akt inhibitors
:MEK inhibitors
B
P > 0.1
P > 0.1
P = 0.01
ZSTK474 (-log GI50) (mol/L)
7.5
7
6.5
6
5.5
GOF(7)
Others(32)
Negative(8)
Positive(31)
Mutant(11)
Wild-type(28)
PIK3CA
PTEN protein
KRAS or BRAF
C
ZSTK474 (-log GI50) (mol/L)
r = 0.44, P = 0.005
0
1
2
3
Phospho-Akt (S473)

database, designated as JFCR39-DB, enabled us to evaluate correlations between the status of pathway members and drug efficacy, as well as correlations among pathway members and among inhibitors *in silico*. First, comparison of the status of pathway members revealed that PTEN loss significantly correlated with upregulated phosphorylation levels of PI3K downstream members and with downregulated phosphorylation levels of Ras downstream members, whereas *KRAS/BRAF* mutation exhibited an opposite tendency. Second, comparison of drug efficacies revealed that most PI3K inhibitors and rapamycins were tightly clustered and were clearly different from other classes of anticancer compounds, suggesting a similarity in the mechanisms of action across these compounds in the cluster. Third, correlation analysis between the status of pathway members and drug efficacy revealed that phosphorylated Akt and *KRAS/BRAF* hotspot mutation correlated with the efficacy and the inefficacy of PI3K inhibitors, respectively. These correlations were confirmed in xenografted human tumors *in vivo*, suggesting that they could serve as predictive biomarkers for PI3K inhibitors.

Correlation analysis among the pathway members revealed that PTEN loss significantly correlated with the phosphorylation levels of Akt, GSK-3β, and TSC2, but *PIK3CA* mutation did not exhibit such correlations, suggesting that PTEN loss was directly connected with activation of these downstream pathway members. Similar results were recently shown by Vasudevan and colleagues using NCI60 cell lines (34) and by Stemke-Hale and colleagues using clinical specimens and cell lines of human breast cancer (35), indicating the significance of PTEN loss in the activation of the PI3K pathway. Furthermore, we showed that PTEN loss was not accompanied by activation of mTOR and S6K1, suggesting the existence of upstream molecule(s) other than Akt that may regulate the activation of mTOR and S6K1. Indeed, mTOR is regulated by energy stress via AMPK and by hypoxia via HIF1α, as well as by growth factor stimulation via PI3K/Akt (13). Interestingly, PTEN loss was strongly associated with inactivation of MAPK pathway components such as MEK1/2 and ERK1/2. Previously, Zimmermann and Moelling reported that phosphorylation of Raf by Akt inhibited activation of the Ras/Raf/MAPK pathway (36), which supports our observation. On the other hand, mutation in either *KRAS* or *BRAF* was strongly correlated with inactivation of PI3K/Akt, rather than activation of the MAPK pathway. This result strongly suggests that gain-of-function mutations of *KRAS* and *BRAF* confer inactivation on Akt and its downstream pathway.

In this study, we performed a mutation analysis of all coding exons of *PIK3CB*, *PIK3CD*, and *PIK3CG* isoforms, which are thought to be rarely mutated in cancer (3). Unexpectedly, we found missense mutations in each isoform that were not registered in the SNP database. Although we could not determine whether they were cancer-specific somatic mutations or derived from germline mutations that have not yet been registered in the SNP database, this is the first report showing that cancer cells harbor missense mutations in these PI3K isoforms. The kinase activities of these mutants compared with their wild-type analogues are under investigation. Cancer cells having these mutations did not exhibit hyperphosphorylation of Akt and its downstream factors, suggesting that they did not activate the canonical PI3K pathway via Akt.

We previously showed that the fingerprints of antitumor compounds across the JFCR39 cell panel can allow evaluation of similarities in the cellular mechanism of action by which drugs exert their antitumor activity (28, 29). Comparison of drug fingerprints revealed that most PI3K inhibitors and rapamycins were tightly clustered and their fingerprints were clearly different from those of other classes of anticancer compounds, suggesting that they act by similar mechanisms, probably by blocking the PI3K/mTOR pathway. Moreover, a fine comparison of the fingerprints of these PI3K pathway inhibitors revealed that ZSTK474 and GDC-0941, both of which are specific class I PI3K inhibitors that do not inhibit other PI3K-related protein kinases including mTOR (15, 37–39), show similar fingerprints ($r = 0.86$). On the other hand, NVP-BEZ235, which is a more potent inhibitor of mTOR than of PI3K (40), exhibited high correlations with the mTOR inhibitor rapamycin ($r = 0.78$), and the correlation was much higher than those with ZSTK474 ($r = 0.67$) and GDC-0941 ($r = 0.46$). Thus, these results suggest that comparison of fingerprints may accurately distinguish the cellular target(s) that determine(s) the susceptibility of cancer cells to these drugs.

Using the integrated PI3K database, we correlated the status of these pathway members with the efficacy of PI3K inhibitors. We first found that either gain-of-function mutation of *PIK3CA* or PTEN loss did not exhibit significant correlation with the efficacy of PI3K inhibitors. Brachmann and colleagues recently reported that NVP-BEZ235 selectively induced apoptosis in *PIK3CA*-mutant breast cancer cells (41). However, in the present study, *PIK3CA*-mutant cell lines did not exhibit hypersensitivity but were susceptible to PI3K inhibitors to a similar extent as those with wild-type *PIK3CA*. Indeed, similar results were obtained in *in vivo* experiments using 24

Figure 3. Fingerprints of 67 compounds including 25 PI3K pathway inhibitors and other conventional anticancer agents and their correlations with the activation status of PI3K pathway members. A, top, the GI_{50} in each cell line was determined and log transformed. The compounds were clustered on the basis of their correlations with other compounds (average-linkage clustered with Pearson correlation metric). Cluster analysis was done by using GeneSpring GX (Agilent Technologies). A yellow point represents the average [log GI_{50}] for each compound across JFCR39. A red point and a blue point represent sensitivity and resistance by 10-fold, respectively. Bottom, a heat map of correlation between the fingerprints of 67 anticancer compounds and those of PI3K pathway members. A red point (high positive Pearson correlation coefficient, $P < 0.001$) indicates that the compound tends to be more effective against cell lines that express more of the protein; a blue point (high negative correlation, $P < 0.001$) indicates the opposite tendency. B, difference in the efficacy of ZSTK474 between cell lines with and without *PIK3CA* gain-of-function mutation, loss of PTEN expression, and *KRAS/BRAF* mutation. C, scatter plots of JFCR39 cell lines showing a significant correlation between phospho-Akt (S473) and the efficacy of ZSTK474.

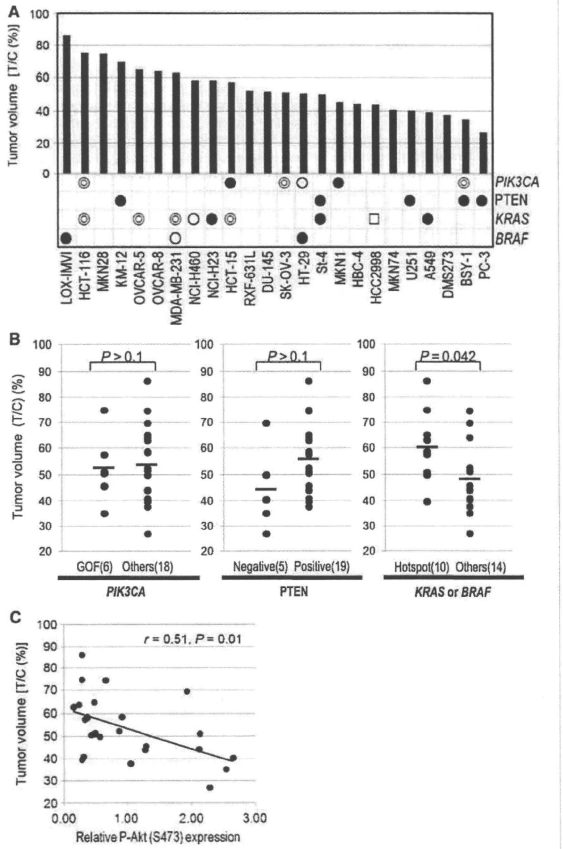

Figure 4. *In vivo* efficacy of ZSTK474 toward human tumors xenografted in nude mice and the activation status of PI3K pathway members. A, 24 transplantable cell lines of JFCR39 were inoculated in nude mice and the *in vivo* efficacy of ZSTK474 (200 mg/kg) was examined (T/C%). The mutation status of *PIK3CA* (closed circle: E545K, double circle: H1047R, open circle: P449T), *PTEN* (closed circle: mutation or deletion without protein expression), *KRAS* (closed circle: G12, double circle: G13, open circle: Q61, open square: A146), and *BRAF* (closed circle: V600E, open circle: G464V) were indicated. B, difference in the *in vivo* efficacy of ZSTK474 between cell lines with and without *PIK3CA* gain-of-function mutation, loss of PTEN expression, and *KRAS/BRAF* hotspot mutation. C, scatter plots of 24 cancer cell lines showing significant correlations between phospho-Akt (S473) expressed in tumor sample and the *in vivo* efficacy of ZSTK474.

transplantable human cancer cell lines xenografted in nude mice (Fig. 4B). We further showed that PI3K inhibitors including ZSTK474 and NVP-BEZ235 inhibit the enzymatic activity of gain-of-function mutant of p110α to an extent comparable to the wild-type (Fig. 1B). These results suggest that such PI3K inhibitors can be used for these cancers. On the other hand, cell lines with mutation in either *KRAS* or *BRAF* exhibited resistance to five PI3K inhibitors including ZSTK474. In *in vivo* studies, we showed that *KRAS/BRAF* mutation exhibited a significant correlation with efficacy of ZSTK474 using 24 xenografted tumors. Similar results were recently reported by Ihle and colleagues by using PX-866 and 13 human tumor xenografts (42) and by Engelman and colleagues using NVP-BEZ235 and a mouse tumor model ectopically expressing a KRAS mutant (23), suggesting the significance of *KRAS/BRAF* mutation in the inefficacy of these PI3K inhibitors.

Of the PI3K pathway downstream members examined in this study, it should be noted that Akt phosphorylated at S473 had significant correlations with 6 of 11 PI3K inhibitors including ZSTK474. Moreover, the correlation between phosphorylated Akt levels and the efficacy of ZSTK474 was confirmed in *in vivo* experiments using 24 human cancer xenografts. This result indicated that the expression level of Akt phosphorylated at S473 could be a candidate biomarker for predicting the efficacy of PI3K inhibitors. The reason why Akt phosphorylated at S473, but not T308, exhibited this correlation is unknown. Phosphorylation of the S473 residue of Akt is known to be catalyzed by the TORC2 complex (whose components include mTOR and rictor) and is required, in addition to T308, for full activation of Akt (43). It is intriguing that the fully activated form of Akt correlated with the efficacy of PI3K inhibitors.

In summary, we constructed an integrated database of PI3K and Ras pathway members and the efficacy of PI3K pathway inhibitors in JFCR39 (JFCR39-DB). *In silico* correlation analysis using JFCR39-DB enabled us to extract two candidates, phospho-Akt and *KRAS/BRAF* mutation, as predictive biomarkers for efficacy of PI3K inhibitors from various pathway members examined. Moreover, we confirmed these correlations by *in vivo* studies using 24 xenografted tumors. The utility of these candidate biomarkers should be validated through clinical studies in future. In addition, JFCR39-DB enabled us to study functional relationships among pathway members and those among drugs. Therefore, JFCR39-DB described here is a useful tool to identify predictive biomarkers, as well as to study the molecular pharmacology of the PI3K pathway in cancer.

Disclosure of Potential Conflicts of Interest

T. Yamori: commercial research grant, Zenyaku Kogyo Co., Ltd. The other authors disclosed no potential conflicts of interest.

Acknowledgments

We thank Yumiko Nishimura and Yoshimi Ohashi for their technical assistance and Zenyaku Kogyo Co. Ltd. for providing us with ZSTK474.

Grant Support

National Institute of Biomedical Innovation, Japan, grant 5-13 (T. Yamori); Grants-in-Aid of the Priority Area "Cancer" from the Ministry of Education, Culture, Sports, Science, and Technology of Japan, nos. 18015049 and 20015048 (T. Yamori); Grants-in-Aid for Scientific Research (B), no. 17390032, and (A), no. 22240092, from the Japan Society for the Promotion of Science (T. Yamori); the Kobayashi Institute for Innovative Cancer Chemotherapy (T. Yamori); and Grants-in-Aid for Young Scientists (B) from the Japan Society for the Promotion of Science, nos. 20790087and 22700929 (S. Dan).

The costs of publication of this article were defrayed in part by the payment of page charges. This article must therefore be hereby marked *advertisement* in accordance with 18 U.S.C. Section 1734 solely to indicate this fact.

Received 11/16/2009; revised 03/25/2010; accepted 04/22/2010; published OnlineFirst 06/08/2010.

References

1. Cantley LC. The phosphoinositide 3-kinase pathway. Science 2002; 296:1655–7.
2. Engelman JA, Luo J, Cantley LC. The evolution of phosphatidylinositol 3-kinases as regulators of growth and metabolism. Nat Rev Genet 2006;7:606–19.
3. Samuels Y, Velculescu VE. Oncogenic mutations of PIK3CA in human cancers. Cell Cycle 2004;3:1221–4.
4. Samuels Y, Wang Z, Bardelli A, et al. High frequency of mutations of the PIK3CA gene in human cancers. Science 2004;304:554.
5. Ma YY, Wei SJ, Lin YC, et al. PIK3CA as an oncogene in cervical cancer. Oncogene 2000;19:2739–44.
6. Shayesteh L, Lu Y, Kuo WL, et al. PIK3CA is implicated as an oncogene in ovarian cancer. Nat Genet 1999;21:99–102.
7. Li J, Yen C, Liaw D, et al. PTEN, a putative protein tyrosine phosphatase gene mutated in human brain, breast, and prostate cancer. Science 1997;275:1943–7.
8. Steck PA, Pershouse MA, Jasser SA, et al. Identification of a candidate tumour suppressor gene, MMAC1, at chromosome 10q23.3 that is mutated in multiple advanced cancers. Nat Genet 1997;15:356–62.
9. Vivanco I, Sawyers CL. The phosphatidylinositol 3-kinase AKT pathway in human cancer. Nat Rev Cancer 2002;2:489–501.
10. Hu L, Zaloudek C, Mills GB, Gray J, Jaffe RB. *In vivo* and *in vitro* ovarian carcinoma growth inhibition by a phosphatidylinositol 3-kinase inhibitor (LY294002). Clin Cancer Res 2000;6:880–6.
11. Ihle NT, Williams R, Chow S, et al. Molecular pharmacology and antitumor activity of PX-866, a novel inhibitor of phosphoinositide-3-kinase signaling. Mol Cancer Ther 2004;3:763–72.
12. Yaguchi S, Fukui Y, Koshimizu I, et al. Antitumor activity of ZSTK474, a new phosphatidylinositol 3-kinase inhibitor. J Natl Cancer Inst 2006;98:545–56.
13. Engelman JA. Targeting PI3K signalling in cancer: opportunities, challenges and limitations. Nat Rev Cancer 2009;9:550–62.
14. Hoeflich KP, O'Brien C, Boyd Z, et al. *In vivo* antitumor activity of MEK and phosphatidylinositol 3-kinase inhibitors in basal-like breast cancer models. Clin Cancer Res 2009;15:4649–64.
15. Kong D, Yamori T. Advances in development of phosphatidylinositol 3-kinase inhibitors. Curr Med Chem 2009;16:2839–54.
16. Ihle NT, Powis G. Take your PIK: phosphatidylinositol 3-kinase inhibitors race through the clinic and toward cancer therapy. Mol Cancer Ther 2009;8:1–9.
17. Knight ZA, Gonzalez B, Feldman ME, et al. A pharmacological map of the PI3-K family defines a role for p110α in insulin signaling. Cell 2006;125:733–47.
18. Liu P, Cheng H, Roberts TM, Zhao JJ. Targeting the phosphoinositide 3-kinase pathway in cancer. Nat Rev Drug Discov 2009;8:627–44.
19. Paez JG, Janne PA, Lee JC, et al. EGFR mutations in lung cancer: correlation with clinical response to gefitinib therapy. Science 2004; 304:1497–500.
20. Lynch TJ, Bell DW, Sordella R, et al. Activating mutations in the epidermal growth factor receptor underlying responsiveness of non-small-cell lung cancer to gefitinib. N Engl J Med 2004;350: 2129–39.
21. Lievre A, Bachet JB, Le Corre D, et al. KRAS mutation status is predictive of response to cetuximab therapy in colorectal cancer. Cancer Res 2006;66:3992–5.
22. Siena S, Sartore-Bianchi A, Di Nicolantonio F, Balfour J, Bardelli A. Biomarkers predicting clinical outcome of epidermal growth factor receptor-targeted therapy in metastatic colorectal cancer. J Natl Cancer Inst 2009;101:1308–24.
23. Engelman JA, Chen L, Tan X, et al. Effective use of PI3K and MEK inhibitors to treat mutant Kras G12D and PIK3CA H1047R murine lung cancers. Nat Med 2008;14:1351–6.
24. Jhawer M, Goel S, Wilson AJ, et al. PIK3CA mutation/PTEN expression status predicts response of colon cancer cells to the epidermal

growth factor receptor inhibitor cetuximab. Cancer Res 2008;68: 1953–61.
25. Sartore-Bianchi A, Martini M, Molinari F, et al. PIK3CA mutations in colorectal cancer are associated with clinical resistance to EGFR-targeted monoclonal antibodies. Cancer Res 2009;69:1851–7.
26. Markman B, Atzori F, Perez-Garcia J, Tabernero J, Baselga J. Status of PI3K inhibition and biomarker development in cancer therapeutics. Ann Oncol 2010;21:683–91.
27. Yamori T, Matsunaga A, Sato S, et al. Potent antitumor activity of MS-247, a novel DNA minor groove binder, evaluated by an *in vitro* and *in vivo* human cancer cell line panel. Cancer Res 1999;59:4042–9.
28. Yamori T. Panel of human cancer cell lines provides valuable database for drug discovery and bioinformatics. Cancer Chemother Pharmacol 2003;52 Suppl 1:S74–9.
29. Shoemaker RH. The NCI60 human tumour cell line anticancer drug screen. Nat Rev Cancer 2006;6:813–23.
30. Paull KD, Shoemaker RH, Hodes L, et al. Display and analysis of patterns of differential activity of drugs against human tumor cell lines: development of mean graph and COMPARE algorithm. J Natl Cancer Inst 1989;81:1088–92.
31. Dan S, Tsunoda T, Kitahara O, et al. An integrated database of chemosensitivity to 55 anticancer drugs and gene expression profiles of 39 human cancer cell lines. Cancer Res 2002;62:1139–47.
32. Sugita H, Dan S, Kong D, Tomida A, Yamori T. A new evaluation method for quantifying PI3K activity by HTRF assay. Biochem Biophys Res Commun 2008;377:941–5.
33. Monks A, Scudiero D, Skehan P, et al. Feasibility of a high-flux anticancer drug screen using a diverse panel of cultured human tumor cell lines. J Natl Cancer Inst 1991;83:757–66.
34. Vasudevan KM, Barbie DA, Davies MA, et al. AKT-independent signaling downstream of oncogenic PIK3CA mutations in human cancer. Cancer Cell 2009;16:21–32.
35. Stemke-Hale K, Gonzalez-Angulo AM, Lluch A, et al. An integrative genomic and proteomic analysis of PIK3CA, PTEN, AKT mutations in breast cancer. Cancer Res 2008;68:6084–91.
36. Zimmermann S, Moelling K. Phosphorylation and regulation of Raf by Akt (protein kinase B). Science 1999;286:1741–4.
37. Kong D, Dan S, Yamazaki K, Yamori T. Inhibition profiles of phosphatidylinositol 3-kinase inhibitors against PI3K superfamily and human cancer cell line panel JFCR39. Eur J Cancer 2010;46:1111–21.
38. Raynaud FI, Eccles SA, Patel S, et al. Biological properties of potent inhibitors of class I phosphatidylinositide 3-kinases: from PI-103 through PI-540, PI-620 to the oral agent GDC-0941. Mol Cancer Ther 2009;8:1725–38.
39. Folkes AJ, Ahmadi K, Alderton WK, et al. The identification of 2-(1*H*-indazol-4-yl)-6-(4-methanesulfonyl-piperazin-1-ylmethyl)-4-morpholin-4-yl-t hieno[3,2-*d*]pyrimidine (GDC-0941) as a potent, selective, orally bioavailable inhibitor of class I PI3 kinase for the treatment of cancer. J Med Chem 2008;51:5522–32.
40. Serra V, Markman B, Scaltriti M, et al. NVP-BEZ235, a dual PI3K/mTOR inhibitor, prevents PI3K signaling and inhibits the growth of cancer cells with activating PI3K mutations. Cancer Res 2008;68: 8022–30.
41. Brachmann SM, Hofmann I, Schnell C, et al. Specific apoptosis induction by the dual PI3K/mTor inhibitor NVP-BEZ235 in HER2 amplified and PIK3CA mutant breast cancer cells. Proc Natl Acad Sci U S A 2009;106:22299–304.
42. Ihle NT, Lemos R, Jr., Wipf P, et al. Mutations in the phosphatidylinositol-3-kinase pathway predict for antitumor activity of the inhibitor PX-866 whereas oncogenic Ras is a dominant predictor for resistance. Cancer Res 2009;69:143–50.
43. Sarbassov DD, Guertin DA, Ali SM, Sabatini DM. Phosphorylation and regulation of Akt/PKB by the rictor-mTOR complex. Science 2005;307:1098–101.

Published OnlineFirst November 9, 2010; DOI:10.1158/0008-5472.CAN-10-0801

Tumor and Stem Cell Biology

Cancer Research

Intrinsic Cooperation between p16^{INK4a} and p21$^{Waf1/Cip1}$ in the Onset of Cellular Senescence and Tumor Suppression *In vivo*

Shinji Takeuchi[1,4,6], Akiko Takahashi[1], Noriko Motoi[2], Shin Yoshimoto[1], Tomoko Tajima[1,3], Kimi Yamakoshi[1], Atsushi Hirao[5], Shigeru Yanagi[3], Kiyoko Fukami[3], Yuichi Ishikawa[2], Saburo Sone[6], Eiji Hara[1], and Naoko Ohtani[1]

Abstract

Although the p16^{INK4a} and p21$^{Waf1/Cip1}$ cyclin-dependent kinase (CDK) inhibitors are known to play key roles in cellular senescence *in vitro*, their roles in senescence remain rather poorly understood *in vivo*. This situation is partly due to the possibility of compensatory effect(s) between p16^{INK4a} and p21$^{Waf1/Cip1}$ or to the upregulation of functionally related CDK inhibitors. To directly address the cooperative roles of p16^{INK4a} and p21$^{Waf1/Cip1}$ in senescence *in vivo*, we generated a mouse line simply lacking both *p16^{INK4a}* and *p21$^{Waf1/Cip1}$* genes [double-knockout (DKO)]. Mouse embryonic fibroblasts (MEF) derived from DKO mice displayed no evidence of cellular senescence when cultured serially *in vitro*. Moreover, DKO MEFs readily escaped Ras-induced senescence and overrode contact inhibition in culture. This was not the case in MEFs lacking either *p16^{INK4a}* or *p21$^{Waf1/Cip1}$*, indicating that p16^{INK4a} and p21$^{Waf1/Cip1}$ play cooperative roles in cellular senescence and contact inhibition *in vitro*. Notably, we found the DKO mice to be extremely susceptible to 7,12-dimethylbenz (*a*)anthracene/12-*O*-tetradecanoylphorbol-13-acetate–induced skin carcinogenesis that involves oncogenic mutation of the *H-ras* gene. Mechanistic investigations suggested that the high incidence of cancer in DKO mice likely reflected a cooperative effect of increased benign skin tumor formation caused by p21$^{Waf1/Cip1}$ loss, with increased malignant conversion of benign skin tumors caused by p16^{INK4a} loss. Our findings establish an intrinsic cooperation between p16^{INK4a} and p21$^{Waf1/Cip1}$ in the onset of cellular senescence and tumor suppression *in vivo*. *Cancer Res; 70(22); 9381–90. ©2010 AACR.*

Introduction

The p16^{INK4a} and p21$^{Waf1/Cip1}$ cyclin-dependent kinase (CDK) inhibitors are known to play key roles in the onset of cellular senescence, a state of permanent cell cycle arrest in culture (1–6). The simultaneous induction of p21$^{Waf1/Cip1}$ and p16^{Ink4a} expression cooperatively blocks the activation of both cyclin D kinase (CDK4/6) and cyclin E kinase (CDK2), allowing the accumulation of the dephosphorylated form of the retinoblastoma tumor suppressor protein (pRb) and thereby causing permanent cell cycle arrest (7–10). It has become apparent that cellular senescence can be induced by a variety of potentially oncogenic stimuli, such as telomere shortening, DNA damage, oxidative stress, or oncogene expression (11–14), suggesting that cellular senescence is likely to act as a tumor suppression mechanism *in vivo* (15, 16). Although the roles of p16^{Ink4a} and p21$^{Waf1/Cip1}$ in cellular senescence are well documented in various cell culture studies, the *in vivo* roles of these CDK inhibitors are poorly understood (17). For example, mice lacking *p16^{INK4a}* (18, 19) or *p21$^{Waf1/Cip1}$* (20–22) exhibit only a little predisposition to spontaneous tumor formation. These observations raise the question of whether the results seen in cell culture studies truly reflect the physiologic roles of these CDK inhibitors *in vivo*. However, it is also possible that these weak phenotypes could be due to functional compensatory effect(s) between p16^{Ink4a} and p21$^{Waf1/Cip1}$.

To directly address the cooperative roles of p16^{INK4a} and p21$^{Waf1/Cip1}$ *in vivo*, we generated a compound mouse line simply lacking both of the *p16^{INK4a}* and *p21$^{Waf1/Cip1}$* genes [double-knockout (DKO) mouse] on a C57BL/6 background, which is known to be carcinogenesis resistant (23–25), and evaluated the roles of these two critical senescence inducers *in vitro* and *in vivo*. Intriguingly, DKO mice are significantly more susceptible to chemical carcinogenesis compared with mice lacking either *p16^{INK4a}* or *p21$^{Waf1/Cip1}$* alone. Moreover, mouse embryonic fibroblasts (MEF) derived from DKO mice

Authors' Affiliations: Divisons of [1]Cancer Biology and [2]Pathology, The Cancer Institute of Japanese Foundation for Cancer Research (JFCR); [3]School of Life Science, Tokyo University of Pharmacy and Life Sciences, Tokyo, Japan; Divisions of [4]Medical Oncology and [5]Molecular Genetics, Cancer Research Institute, Kanazawa University, Kanazawa, Japan; and [6]Institute of Health Biosciences, University of Tokushima, Tokushima, Japan

Note: Supplementary data for this article are available at Cancer Research Online (http://cancerres.aacrjournals.org/).

Corresponding Author: Naoko Ohtani, Division of Cancer Biology, The Cancer Institute of Japanese Foundation for Cancer Research (JFCR), Tokyo 135-8550, Japan. Phone: 81-3-3570-0605; Fax: 81-3-3570-0457; E-mail: naoko.ohtani@jfcr.or.jp.

doi: 10.1158/0008-5472.CAN-10-0801

Published OnlineFirst November 9, 2010; DOI:10.1158/0008-5472.CAN-10-0801

are resistant to the onset and the maintenance of cellular senescence in culture. These results indicate that $p16^{INK4a}$ plays a critical role in cooperating with $p21^{Waf1/Cip1}$ in tumor suppression *in vivo*.

Materials and Methods

Generation of $p16^{-/-}$:$p21^{-/-}$ mice

$p16^{-/-}$ mice (C57BL/6) were kindly provided by N.E. Sharpless (University of North Carolina Lineberger Comprehensive Cancer Center, Chapel Hill, NC; ref. 19). *$p21^{-/-}$* mice (C57BL/6) were kindly provided by P. Leder (Harvard Medical School, Boston, MA; ref. 20). *$p16^{-/-}$:$p21^{-/-}$* DKO mice were generated by crossing *$p16^{-/-}$* mice and *$p21^{-/-}$* mice. All animals were cared for by using protocols approved by the Committee for the Use and Care of Experimental Animals of the Japanese Foundation for Cancer Research.

Cell culture

MEFs were generated from E13.5 embryos of wild-type, *$p16^{-/-}$*, *$p21^{-/-}$*, or *$p16^{-/-}$:$p21^{-/-}$* DKO mice as previously described (26). MEFs were grown in DMEM supplemented with 10% fetal bovine serum in 3% O_2/5% CO_2 for 2 days, harvested, viably frozen, and labeled as passage 0. Serial 3T3 cultivation was done as described (27). Cells were counted in triplicate. The number of cells present on the third day (N3) was divided by the initial cell number (N0 = 3×10^5) and plotted as growth rate (N3/N0; Supplementary Fig. S1). The increase in the population doubling level (ΔPDL) was calculated according to the following formula: ΔPDL = log (Nf/N0)/log 2, where N0 is the initial number of cells (3×10^5) and Nf is the final number of cells.

Western blot analysis

Proteins (40 μg) were analyzed by Western blotting, as previously described (6). The primary antibodies used were $p16^{INK4a}$ (11104 IBL), $p21^{Waf1/Cip1}$ (sc-6246, Santa Cruz Biotechnology, Inc.), $p15^{INK4b}$ (sc-613, Santa Cruz Biotechnology), p53 (1C12, Cell Signaling), $p19^{Arf}$ [ab80 (Abcam) or sc-32748 (Santa Cruz Biotechnology)], H-Ras (sc-29, Santa Cruz Biotechnology), pRb (554136, BD Pharmingen), β-actin (AC-74, Sigma-Aldrich), and α-tublin (DM-1A, Sigma-Aldrich). Secondary antibodies were detected by enhanced chemiluminescence (Amersham).

Retrovirus infection and focus formation assay

Retroviral gene transfer was done by transient transfection of the LinxE ecotropic packaging cells with a pBabe-puro vector and the vector containing the human H-rasV12 oncogene, as previously described (6). Forty-eight hours after transfection, the retrovirus-containing medium was collected, filtered, supplemented with 8 μg/mL polybrene (Sigma), and used for multiple infection (twice a day for 2 days) into early-passage MEFs (P0–P1) growing in 3% O_2/5% CO_2. Infected cell populations were selected for 5 days in the presence of 1 μg/mL puromycin. For foci formation assays, 1.7×10^4 puromycin-selected immortalized cells were seeded into 6-cm-diameter dishes. Cells were maintained for 15 days in a 3% O_2/5% CO_2 culture environment, and the medium was changed twice a week until the cells were photographed and counted.

Senescence-associated β-galactosidase assay

Senescence-associated β-galactosidase assay was done as described previously (28).

Analysis of intracellular reactive oxygen species

To assess the generation of intracellular levels of reactive oxygen species (ROS), cells were incubated with 20 μmol/L 2′,7′-dichlorofluorescein diacetate (Calbiochem) for 20 minutes at 37°C. The peak excitation wavelength for oxidized 2′,7′-dichlorofluorescein was 488 nm and the emission wavelength was 525 nm as described previously (6).

Chemically induced skin tumor formation

The chemically induced skin tumor formation analysis was done as described previously (29). Briefly, mice of the wild-type, p16-KO, p21-KO, or DKO genotypes in the resting phase of the hair cycle (8 weeks old) were shaved and treated with 100 μg of 7,12-dimethylbenz(*a*)anthracene (DMBA) in 100 μL of acetone. One week after DMBA treatment, mice were subsequently treated twice a week with 12.5 μg of 12-*O*-tetradecanoylphorbol-13-acetate (TPA) in 100 μL of acetone for 20 weeks. Tumors developed in mice were analyzed for histology at 30 weeks after DMBA treatment.

Histologic analysis

Tissues were fixed in 10% buffered formalin, progressively dehydrated through gradients of alcohol, and embedded in paraffin. Samples were sectioned on a microtome at 4-μm thickness, deparaffinized in xylene, rehydrated, and then stained with H&E for histologic analysis.

Results

$p16^{INK4a}$:$p21^{Waf1/Cip1}$ DKO MEFs proliferate without any induction of cellular senescence by serial passaging

Compound mice lacking both *$p16^{INK4a}$* and *$p21^{Waf1/Cip1}$* on a C57BL/6 background (DKO mice) are fertile and born normally in the expected Mendelian ratio. MEFs derived from wild-type mice, *$p16^{INK4a}$* knockout (p16-KO) mice, *$p21^{Waf1/Cip1}$* knockout (p21-KO) mice, and DKO mice were subjected to serial passage using the 3T3 protocol under standard culture conditions, which included atmospheric (20%) oxygen. Consistent with previous reports, p16-KO MEFs underwent cellular senescence in a kinetic pattern similar to that of wild-type MEFs (Fig. 1A; Supplementary Fig. S1A and C; refs. 18, 19). The level of $p15^{INK4b}$ expression was remarkably increased and the $p21^{Waf1/Cip1}$ level remained high in senescent p16-KO MEFs, implying that a compensatory network among the CDK inhibitors indeed exists as previously suggested (refs. 30–33; Fig. 1C, lanes 1–4 and 10–13). p21-KO MEFs proliferated without detectable senescence growth arrest, although they exhibited a slight reduction in proliferation rate at passage 4, as previously reported (ref. 26; Fig. 1A; Supplementary Fig. S1A

Published OnlineFirst November 9, 2010; DOI:10.1158/0008-5472.CAN-10-0801

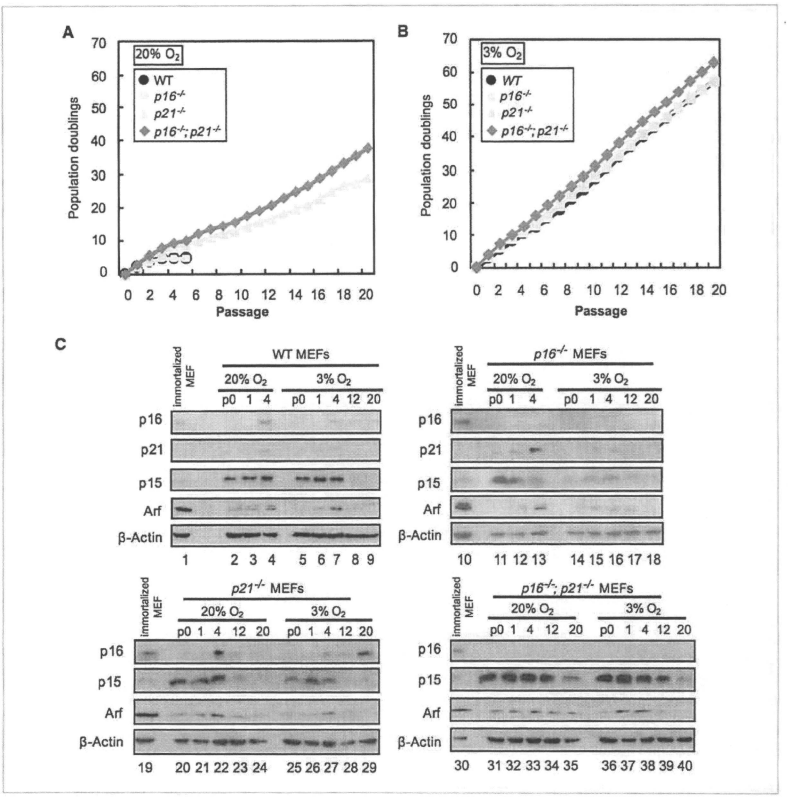

Figure 1. Serial 3T3 cultivation of primary MEFs of different genotypes. A and B, MEFs derived from wild-type (WT), p16-KO, p21-KO, and DKO mice were cultivated according to the 3T3 protocol. The graphs represent the accumulated population doublings at every passage (A, in 20% oxygen; B, in 3% oxygen). The means ± SD of triplicate experiments are shown. C, protein levels of the cell cycle inhibitors $p16^{INK4a}$, $p21^{Waf1/Cip1}$, $p15^{INK4b}$, and $p19^{Arf}$. Note that passage 20 of the wild-type and p16-KO MEFs in 20% oxygen culture could not be analyzed because a very long period of time was required to generate an immortalized culture. To compare the levels of proteins across the gels, the same sample (immortalized MEFs) was loaded on every gel (lanes 1, 10, 19, and 30). β-Actin was used as a loading control. Representative data of two independent experiments are shown. Uncropped images are shown in Supplementary Data.

and C). Interestingly, MEFs lacking both $p16^{INK4a}$ and $p21^{Waf1/Cip1}$ (DKO MEFs) grew slightly but consistently better than p21-KO MEFs, suggesting that $p16^{INK4a}$ also plays a role, at least to some extent, in the cellular senescence provoked by the serial passage of MEFs (Fig. 1A; Supplementary Fig. S1A).

Because primary MEFs have been shown to be exquisitely sensitive to oxidative stress in culture (34), we next cultured these MEFs with 3% oxygen, which is known to be similar to the physiologic oxygen condition *in vivo* (34). In contrast to the result with the 20% oxygen condition, we were unable to see any significant difference in the cell proliferation rate between wild-type MEFs and MEFs lacking the $p16^{INK4a}$ or $p21^{Waf1/Cip1}$ gene (Fig. 1B; Supplementary Fig. S1B and D), although the DKO MEFs proliferated

Published OnlineFirst November 9, 2010; DOI:10.1158/0008-5472.CAN-10-0801

slightly better than the MEFs of other types (Fig. 1B; Supplementary Fig. S1B). As seen in the 20% oxygen condition, the level of $p15^{INK4b}$ expression, but not the expression of the other $p16^{INK4a}$ family members (data not shown), was substantially increased in both p16-KO MEFs and DKO MEFs under the 3% oxygen condition (Fig. 1C, lanes 1–18 and 30–40), suggesting that $p15^{INK4b}$ may play a compensatory role in the absence of $p16^{INK4a}$ regardless of the oxygen conditions *in vitro*, although this level of $p15^{INK4b}$ expression does not seem to be high enough to block cell proliferation (Fig. 1B; Supplementary Fig. S1B). Furthermore, because the *p19*^{Arf} gene shares a locus with *p16*^{INK4a} and is also implicated in tumor suppression (35, 36), we examined the level of $p19^{Arf}$ in these MEFs. However, we did not see any substantial difference in $p19^{Arf}$ expression in MEFs lacking the *p16*^{INK4a} and/or *p21*$^{Waf1/Cip1}$ gene compared with wild-type MEFs (Fig. 1C).

DKO MEFs expressing oncogenic Ras escape contact inhibition and form foci

Because cellular senescence can also be induced by activated *ras* oncogene expression, we next asked if the status of the *p16*^{INK4a} and/or *p21*$^{Waf1/Cip1}$ gene affects Ras-induced senescence under physiologic (3%) oxygen conditions. In contrast to passage-induced senescence, MEFs of all the genotypes exhibited features of cellular senescence, including cell cycle arrest, a flat and enlarged morphology, and the accumulation of the dephosphorylated form of pRb within 10 days of infection with retrovirus encoding oncogenic Ras (Fig. 2). Notably, increased expression of $p15^{INK4b}$ as well as p53 and $p19^{Arf}$ upregulation was observed in Ras-induced senescence (Fig. 2D). The depletion of $p15^{INK4b}$ by small interference RNA abrogated the appearance of senescence markers in Ras-infected DKO MEFs (Supplementary Fig. S2). It is therefore likely that the upregulation of $p15^{INK4b}$ expression plays an important role, at least partly, in oncogenic Ras–induced senescence in DKO MEFs. However, although the levels of senescence-associated β-galactosidase activity (Fig. 2B) and the intracellular levels of ROS (Fig. 2C), which are markers of cellular senescence, were increased in DKO MEFs, the level of induction was less evident compared with the MEFs of other genotypes. These results raise the possibility that $p16^{INK4a}$ and $p21^{Waf1/Cip1}$ are both required for the full induction of oncogenic Ras–induced senescence in culture. Indeed, DKO MEFs expressing oncogenic Ras readily escaped the senescent state and reinitiated proliferation more rapidly than the MEFs of other genotypes under the 3% oxygen condition (Fig. 3A). Note that the saturation density of the DKO MEFs expressing oncogenic Ras was remarkably higher than that of the other cell types (Fig. 3B). Interestingly, significant numbers of foci were also observed in the confluent culture of the DKO MEFs expressing oncogenic Ras, but not the MEFs of other genotypes, under the 3% oxygen condition (Fig. 3C). Taken together, these results suggest that oncogenic Ras expression, in conjunction with the loss of $p16^{INK4a}$ and $p21^{Waf1/Cip1}$, may have potential to counteract the pathway involved in contact inhibition in cultured MEFs.

DKO mice are extremely susceptible to DMBA/TPA–induced skin cancer

To explore the role of $p16^{INK4a}$ and $p21^{Waf1/Cip1}$ in oncogenic Ras expression in a more physiologic setting, wild-type, p16-KO, p21-KO, and DKO mice were subjected to a conventional chemically induced skin carcinogenesis protocol, with a single dose of DMBA followed by biweekly treatment of TPA for 20 weeks. Because this protocol is known to cause an oncogenic mutation in the endogenous *H-ras* gene, it seemed to be an ideal system for studying the physiologic response to oncogenic Ras expression in living animals (37). In p16-KO mice, the frequency of benign skin papilloma formation was not increased, and the maximum number of papillomas was 6.8 per mouse on average, whereas 6.0 papillomas developed in wild-type mice (Fig. 4A and B). Interestingly, however, 23.08% of the p16-KO mice developed at least one malignant skin tumor (Fig. 4B; Table 1), whereas 5.56% of the wild-type mice developed skin cancer (Fig. 4A; Table 1) at 30 weeks after DMBA treatment. Note that a malignant tumor that appeared in the wild-type mice was carcinoma *in situ*, whereas two thirds of the malignant tumors in the p16-KO mice were more aggressive and invasive cancers (Table 1). The malignant conversion ratio from benign papillomas in p16-KO mice was approximately five times higher than that in wild-type mice (0.93% in wild-type mice versus 4.55% in p16-KO mice; see Table 1), indicating that $p16^{INK4a}$ plays a role in preventing the malignant conversion of benign skin tumors, but not benign skin tumor formation itself, at least in this setting. This is consistent with the observation that $p16^{INK4a}$ expression is upregulated in the late stage (30 weeks after DMBA treatment), but not in the early stage (10 weeks after DMBA treatment), of DMBA/TPA–induced skin papillomas (Supplementary Fig. S3; ref. 29). In addition, the level of $p19^{Arf}$ expression was also increased in the late papillomas (Supplementary Fig. S3), as seen in Ras-induced senescence in cultured MEFs (Fig. 2D). These results suggest that the upregulation of $p19^{Arf}$, at least in part, contributes to the induction of Ras-induced senescence *in vitro* and *in vivo* in mice.

In stark contrast with p16-KO mice, the frequency of benign skin papilloma formation was strikingly increased in p21-KO mice (the maximum number was 12.5 papillomas per mouse; Fig. 4C). However, surprisingly, the malignant conversion rate to advanced cancers was not increased in these p21-KO mice (1.23%) at 30 weeks after DMBA treatment in this setting (Table 1). These results are consistent with the previous observation by Weinberg and colleagues (38), but not with the report by Topley and colleagues (39). However, because each group used different protocols and mouse strains, these seemingly contradictory data are, at least partly, due to the differences in the experimental conditions between our study and the study of Topley and colleagues (39). Nevertheless, a substantial level of $p21^{Waf1/Cip1}$ expression, but not $p16^{INK4a}$ expression, was induced in the early stage of the benign skin papillomas (10 weeks after DMBA treatment; Supplementary Fig. S3). These data imply that a major role of $p21^{Waf1/Cip1}$ is likely to be preventing benign skin papilloma formation rather than the

Published OnlineFirst November 9, 2010; DOI:10.1158/0008-5472.CAN-10-0801

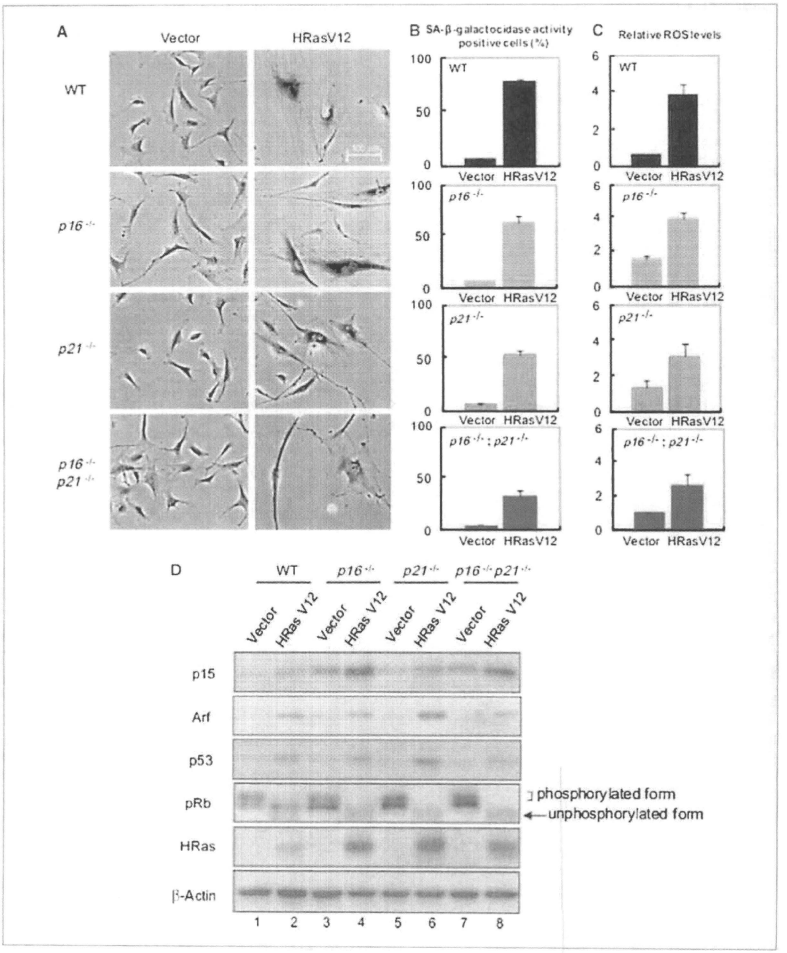

Figure 2. Induction of oncogene-induced cellular senescence by retrovirally transduced oncogenic Ras in wild-type, p16-KO, p21-KO, and DKO MEFs. MEFs of the indicated genotypes were infected with control retrovirus or retrovirus encoding oncogenic Ras, and a series of experiments were performed a week after infection. A, representative photographs of cells; B, percentage of senescence-associated β-galactosidase (SA-β-gal) positive MEFs; C, relative ROS levels. Columns, mean of three independent experiments; bars, SD. D, protein levels of $p15^{INK4B}$, $p19^{Arf}$, p53, Rb, and H-Ras in MEFs infected with retrovirus encoding oncogenic Ras (H-RasV12) or control empty vector (Vector). β-Actin was used as a loading control. Representative data of two independent experiments are shown. Uncropped images are shown in Supplementary Data.

Published OnlineFirst November 9, 2010; DOI:10.1158/0008-5472.CAN-10-0801

malignant conversion of benign skin tumors, at least in this setting, although it is also possible that $p21^{Waf1/Cip1}$ may have the ability to block progression to higher-grade benign papillomas.

It is interesting that the frequencies of both the benign papilloma formation (the maximum number was 16.0 papillomas per mouse) and the incidence of cancer-bearing mice were dramatically enhanced when DKO mice were subjected to the DMBA/TPA–induced skin carcinogenesis protocol (Fig. 4D; Table 1). By 30 weeks after the DMBA/TPA treatment, 84.21% of the DKO mice developed at least one carcinoma (Fig. 4D; Table 1). Notably, however, the malignant

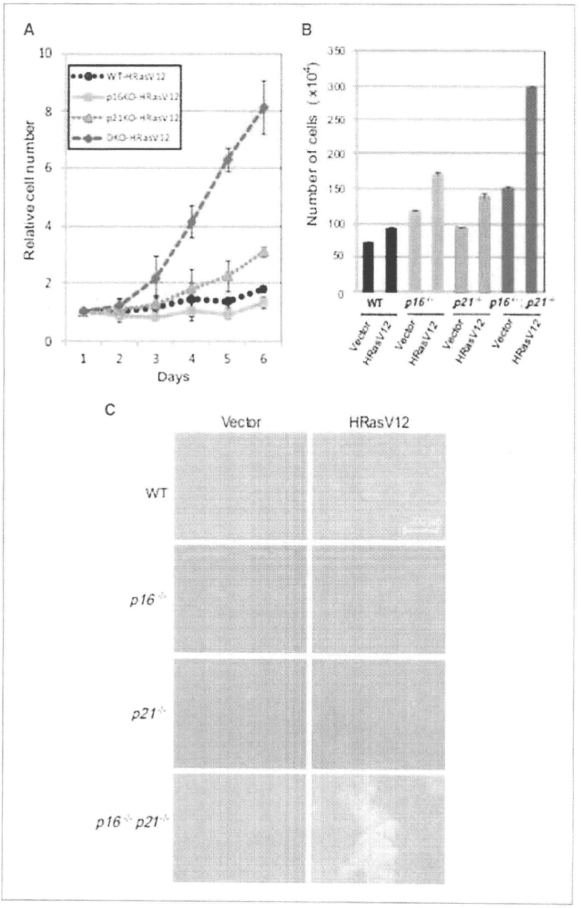

Figure 3. DKO MEFs escape contact inhibition. A, the cell numbers of wild-type, p16-KO, p21-KO, and DKO MEFs expressing oncogenic Ras were counted 7 d after retrovirus infection (indicated as day 1). The cells were counted in triplicate and the relative cell numbers are shown. B, relative cell numbers of wild-type, p16-KO, p21-KO, and DKO MEFs expressing oncogenic Ras in the focus formation assay. The means ± SD of triplicate experiments are shown. C, Ras-expressing immortalized DKO MEFs, but not the MEFs of other genotypes, formed foci after 15 d of culture. Representative data of three independent experiments are shown.

Published OnlineFirst November 9, 2010; DOI:10.1158/0008-5472.CAN-10-0801

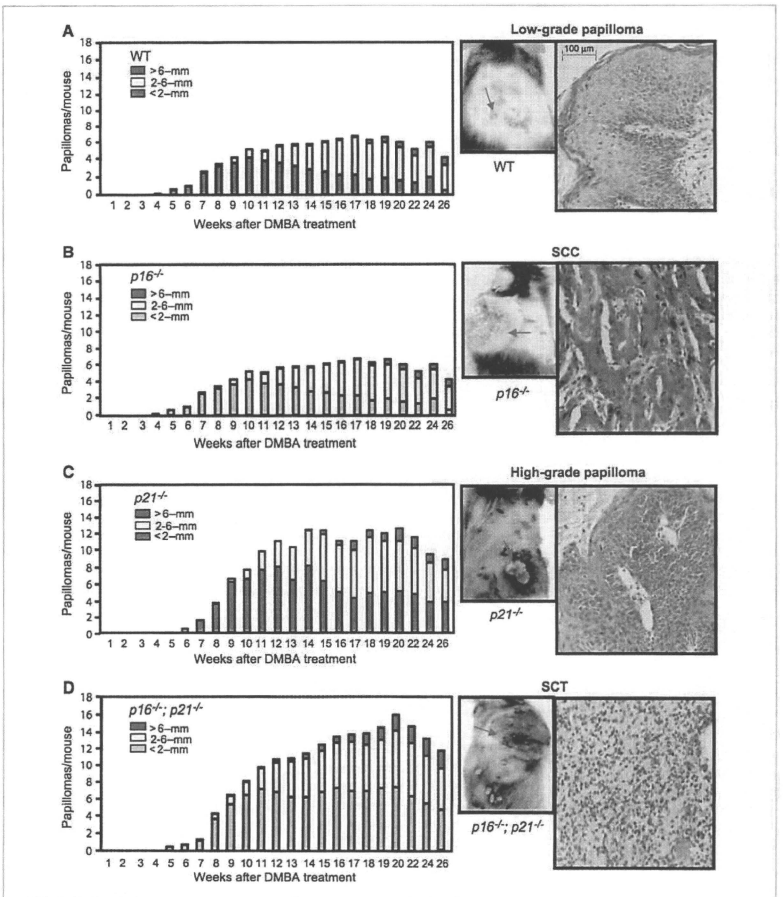

Figure 4. Analysis of DMBA/TPA–induced skin tumors. A to D, wild-type (n = 18; A), p16-KO (n = 13; B), p21-KO (n = 13; C), and DKO (n = 19; D) mice. Left, average number of papillomas at the indicated times and their relative size distribution. Middle, representative images of skin tumors at 30 wk after DMBA treatment. Right, histology of the representative tumors (indicated by red arrows in the tumor images; H&E staining; magnification, ×100). A, a low-grade papilloma showing thickening of epidermis with slight cellular atypia mainly in the parabasal layer and with hyperkeratosis. B, a large tumor with ulceration in the center of the tumor. Histologically, the tumor is diagnosed as squamous cell carcinoma (SCC) showing papillary proliferation of atypical epidermal cells with dyskeratosis. C, a high-grade papilloma showing papillary proliferation of the epidermis with cellular atypia, including high nucleus/cytoplasm (N/C) ratio, increase of nuclear chromatin, and increase of mitotic figures, although the polarity of maturation is still preserved. D, a spindle cell tumor (SCT), not otherwise specified, which showed diffuse proliferation of relatively uniform short spindle cells. Yellow arrows, muscle layers. Representative results of two independent experiments are shown.

Published OnlineFirst November 9, 2010; DOI:10.1158/0008-5472.CAN-10-0801

conversion rate of benign papillomas in DKO mice (5.92%) was not increased compared with that in p16-KO mice (4.55%; Table 1). These results indicate that the high incidence of cancer in the mice with the DKO genotype is likely to be due to a cooperative effect of increased benign skin papilloma formation due to $p21^{Waf1/Cip1}$ loss and increased malignant conversion of benign skin tumors due to $p16^{INK4a}$ loss. It is also worth emphasizing that 31.6% (6 of 19) of the DKO mice developed malignant spindle cell tumors, which were more aggressively invasive through the muscle layers compared with squamous cell carcinomas (Fig. 4D; Table 1).

An intact DNA damage response prevents the progression of DMBA/TPA–induced skin tumors

It was reported that oncogenic Ras induces DNA damage signaling and the activation of the cell cycle checkpoint, which are critical for the cellular senescence and tumor suppression phenotypes (40–42). Therefore, we have examined γ-H2AX foci formation, a DNA damage response marker, in tumors in all the genotypes. γ-H2AX foci were detectable in a significant percentage of cells in the low-grade papillomas in the wild-type, p21-KO, and p16-KO mice. In contrast, a very small percentage of cells were positive for γ-H2AX foci in the low-grade papillomas that developed in DKO mice (Supplementary Fig. S4). These results suggest that $p21^{Waf1/Cip1}$ and $p16^{INK4a}$ play important roles in conducting the DNA damage signaling pathway. Note that γ-H2AX foci were hardly detectable in most of the high-grade papillomas and malignant tumors, such as squamous cell carcinomas and spindle cell tumors, regardless of the genotype, suggesting that the higher-grade papillomas and the malignant tumors seem to have a defect in responding to DNA damage signals.

Discussion

In this study, we have generated for the first time the $p16^{INK4a}$;$p21^{Waf1/Cip1}$ double mutant mice (DKO mice) on a C57BL/6 background, a carcinogenesis-resistant strain, and analyzed the effects of $p16^{INK4a}$ and $p21^{Waf1/Cip1}$ deficiency on the susceptibility to cancer in cooperation with oncogenic Ras expression. MEFs derived from DKO mice easily escaped Ras-induced senescence and overrode contact inhibition in culture (Fig. 3). Moreover, DKO-mice on the C57BL/6 background were extremely susceptible to DMBA/TPA–induced skin carcinogenesis (Fig. 4). Our analyses clearly show a significant increase of cancer incidence in the DKO background because $p21^{Waf1/Cip1}$ deletion promotes benign skin tumor development and $p16^{INK4a}$ deletion promotes the incidence of malignant conversion of benign skin tumors (Table 1).

There are reports showing that compound mice expressing a mutant form of CDK4 (CDK4-R24C), which is resistant to all of the $p16^{INK4a}$ family members, on a $p21^{Waf1/Cip1}$-null background are more susceptible to malignant tumors compared with mice either lacking $p21^{Waf1/Cip1}$ or expressing *CDK4-R24C* (27, 43). However, because CDK4-R24C has the ability to counteract all of the $p16^{INK4a}$ family members, it has been unclear whether $p16^{INK4a}$ or other $p16^{INK4a}$ family members play a role in cooperating with $p21^{Waf1/Cip1}$ in the induction of cellular senescence and/or tumor suppression *in vivo*. Our study has clarified that the increased tumor incidence and immortalization of the previously described *cdk4r24c* mutant mice and MEFs with the $p21^{Waf1/Cip1}$-null background are most likely to be due to the absence of $p16^{INK4a}$ from among the INK4 family both *in vitro* and *in vivo*.

It is also noteworthy that 31.6% of the DKO mice developed malignant spindle cell tumors, which were more aggressive

Table 1. Skin tumor susceptibility by DMBA/TPA in p16 and/or p21 knockout mice

	Mouse genotype			
	Wild-type (n = 18)	$p16^{-/-}$ (n = 13)	$p21^{-/-}$ (n = 13)	$p16^{-/-}$;$p21^{-/-}$ (n = 19)
Tumor type, n*				
Low-grade papilloma	16	5	4	2
High-grade papilloma	1	5	7	1
High-grade papilloma with microinvasion	0	0	2	1
Carcinoma *in situ*	1	1	0	1
Squamous cell carcinoma	0	2	0	8
Malignant spindle cell tumor	0	0	0	6
Mice with carcinomas, %	5.56	23.08	15.38	84.21
Maximum no. of papillomas/mouse	6.0	6.8	12.5	16.0
Malignant conversion ratio at 30 wk after DMBA (no. of carcinomas/total no. of papillomas), %	0.93	4.55†	1.23	5.92‡

NOTE: Tumors were analyzed 30 wk after DMBA treatment.
*The number of mice with the indicated tumors is shown.
†One $p16^{-/-}$ mouse harbored two SCCs.
‡Two $p16^{-/-}$;$p21^{-/-}$ mice harbored two SCCs.

Published OnlineFirst November 9, 2010; DOI:10.1158/0008-5472.CAN-10-0801

than squamous cell carcinomas (Fig. 4D; Table 1). It is interesting that all of these spindle cell tumors exhibited a substantial increase in the expression of the *Oct4* gene, which is known to play an important role in stem cell maintenance and reprogramming (Supplementary Fig. S5), although the molecular mechanism behind this upregulation remains unclear. This is consistent in part with recent reports showing that both the $p16^{INK4a}$ and $p53\text{-}p21^{Waf1/Cip1}$ pathways play an inhibitory role in the reprogramming of differentiated cells toward becoming induced pluripotent stem cells (44–49). It is therefore tempting to speculate that the inactivation of both $p16^{Ink4a}$ and $p21^{Waf1/Cip1}$, in conjunction with Ras activation, increases the chance of reprogramming differentiated cells or stimulates the proliferation of undifferentiated cells *in vivo*. Further analysis is required to understand how the $p16^{Ink4a}$ and $p21^{Waf1/Cip1}$ pathways are linked to Oct4 expression.

It is still possible that the phenotypic effects seen in $p16^{INK4a}$ knockout mice and DKO mice are compromised, at least to some extent, by developmental or somatic compensation by upregulation of the remaining $p16^{INK4a}$ family members (30–33). Nonetheless, our results provide direct evidence that $p16^{Ink4a}$ and $p21^{Waf1/Cip1}$ play cooperative roles in the onset and/or the maintenance of Ras-induced senescence *in vitro* and show for the first time that $p16^{INK4a}$ per se plays a crucial role in preventing the malignant conversion of benign skin tumors *in vivo*.

Disclosure of Potential Conflicts of Interest

No potential conflicts of interest were disclosed.

Acknowledgments

We thank Dr. P. Leder for $p21^{Waf1/Cip1}$-knockout mice, Dr. N.E. Sharpless for $p16^{INK4a}$-knockout mice, and Dr. M. Serrano [Spanish National Cancer Research Center (CNIO), Madrid, Spain] for retrovirus vector encoding H-RasV12. We also thank C. Sugita and S. Ohtomi for their assistance in mouse experiments.

Grant Support

Ministry of Education, Science, Sports and Technology of Japan, the Astellas Foundation for Research on Metabolic Disorders, the Vehicle Racing Commemorative Foundation, the Takeda Science Foundation, the Uehara Memorial Foundation, and the Mishima Kaiun Memorial Foundation.

The costs of publication of this article were defrayed in part by the payment of page charges. This article must therefore be hereby marked *advertisement* in accordance with 18 U.S.C. Section 1734 solely to indicate this fact.

Received 03/05/2010; revised 08/11/2010; accepted 09/15/2010; published OnlineFirst 11/09/2010.

References

1. Noda A, Ning Y, Venable SF, Pereira-Smith OM, Smith JR. Cloning of senescent cell-derived inhibitors of DNA synthesis using an expression screen. Exp Cell Res 1994;211:90–8.
2. Hara E, Smith R, Parry D, Tahara H, Stone S, Peters G. Regulation of $p16^{CDKN2}$ expression and its implications for cell immortalization and senescence. Mol Cell Biol 1996;16:859–67.
3. Alcorta DA, Xiong Y, Phelps D, Hannon G, Beach D, Barrett JC. Involvement of the cyclin-dependent kinase inhibitor $p16^{INK4a}$ in replicative senescence of normal human fibroblasts. Proc Natl Acad Sci U S A 1996;93:13742–7.
4. Serrano M, Lin AW, McCurrach ME, Beach D, Lowe SW. Oncogenic ras provokes premature cell senescence associated with accumulation of p53 and $p16^{INK4a}$. Cell 1997;88:593–602.
5. Randle DH, Zindy F, Sherr CJ, Roussel MF. Differential effects of $p19^{Arf}$ and $p16^{Ink4a}$ loss on senescence of murine bone marrow-derived preB cells and macrophages. Proc Natl Acad Sci U S A 2001;98:9654–9.
6. Takahashi A, Ohtani N, Yamakoshi K, et al. Mitogenic signalling and the $p16^{INK4a}$-Rb pathway cooperate to enforce irreversible cellular senescence. Nat Cell Biol 2006;8:1291–7.
7. McConnell BB, Gregory FJ, Stott FJ, Hara E, Peters G. Induced expression of $p16^{INK4a}$ inhibits both CDK4- and CDK2-associated kinase activity by reassortment of cyclin-CDK-inhibitor complexes. Mol Cell Biol 1999;19:1981–9.
8. Mitra J, Dai CY, Somasundaram K, et al. Induction of $p21^{WAF1/CIP1}$ and inhibition of Cdk2 mediated by the tumor suppressor $p16^{INK4a}$. Mol Cell Biol 1999;19:3916–28.
9. Sherr CJ, Roberts JM. CDK inhibitors: positive and negative regulators of G_1-phase progression. Genes Dev 1999;13:1501–12.
10. Li W, Kotoshiba S, Berthet C, Hilton MB, Kaidis P. Rb/Cdk2/Cdk4 triple mutant mice elicit an alternative mechanism for regulation of the G_1-S transition. Proc Natl Acad Sci U S A 2009;106:486–91.
11. Collado M, Blasco MA, Serrano M. Cellular senescence in cancer and aging. Cell 2007;130:223–33.
12. Jacobs JJ, de Lange T. $p16^{INK4a}$ as a second effector of the telomere damage pathway. Cell Cycle 2005;4:1364–8.
13. Ben-Porath I, Weinberg RA. When cells get stressed: an integrative view of cellular senescence. J Clin Invest 2004;113:8–13.
14. Okada H, Mak TW. Pathways of apoptotic and non-apoptotic death in tumor cells. Nat Rev Cancer 2004;4:592–603.
15. Sharpless NE, DePinho RA. Cancer: crime and punishment. Nature 2005;436:636–7.
16. Campisi J. Senescent cells, tumor suppression, and organismal aging: good citizens, bad neighbors. Cell 2005;F120:513–22.
17. Pei XH, Xiong Y. Biochemical and cellular mechanisms of mammalian CDK inhibitors: a few unresolved issues. Oncogene 2005; 24:2787–95.
18. Krimpenfort P, Quon KC, Mooi WJ, Loonstra A, Berns A. Loss of $p16^{INK4a}$ confers susceptibility to metastatic melanoma in mice. Nature 2001;413:83–6.
19. Sharpless NE, Bardeesy N, Lee KH, et al. Loss of $p16^{INK4a}$ with retention of $p19^{Arf}$ predisposes mice to tumorigenesis. Nature 2001; 413:86–91.
20. Deng C, Zhang P, Harper JW, Elledge SJ, Leder P. Mice lacking $p21^{Waf1/Cip1}$ undergo normal development, but are defective in G_1 checkpoint control. Cell 1995;82:675–84.
21. Brugarolas J, Chandrasekaran C, Gordon JI, Beach D, Jacks T, Hannon GJ. Radiation-induced cell cycle arrest compromised by p21 deficiency. Nature 1995;377:552–7.
22. Martin-Caballero J, Flores JM, García-Palencia P, Serrano M. Tumor susceptibility of $p21^{Waf1/Cip1}$-deficient mice. Cancer Res 2001;61: 6234–8.
23. DiGiovanni J, Prichett WP, Decina PC, Diamond L. DBA/2 mice are as sensitive as SENCAR mice to skin tumor promotion by 12-O-tetradecanoylphorbol-13-acetate. Carcinogenesis 1984;5:1493–8.
24. Hennings H, Glick AB, Lowry DT, Krsmanovic LS, Sly LM, Yuspa SH. FVB/N mice: an inbred strain sensitive to the chemical induction of squamous cell carcinomas in the skin. Carcinogenesis 1993;14: 2353–8.
25. Woodworth CD, Michael E, Smith L, et al. Strain-dependent differences in malignant conversion of mouse skin tumors is an inherent property of the epidermal keratinocyte. Carcinogenesis 2004;25: 1771–8.
26. Pantoja C, Serrano M. Murine fibroblasts lacking p21 undergo senescence and are resistant to transformation by oncogenic Ras. Oncogene 1999;18:4974–82.